Monolithic integration of high electron mobility InAs-based heterostructure on exact (001) silicon using a GaSb/GaP accommodation layer

L. Desplanque, S. El Kazzi, Christophe Coinon, S. Ziegler, B. Kunert, A. Beyer, K. Volz, W. Stolz, Y. Wang, P. Ruterana, et al.

Monolithic integration of high electron mobility InAs-based heterostructure on exact (001) Silicon using a GaSb/GaP accommodation layer

Cite as: Appl. Phys. Lett. **101**, 142111 (2012); https://doi.org/10.1063/1.4758292
Submitted: 06 July 2012 • Accepted: 26 September 2012 • Published Online: 05 October 2012

L. Desplanque, S. El Kazzi, C. Coinon, et al.

Monolithic integration of high electron mobility InAs-based heterostructure on exact (001) Silicon using a GaSb/GaP accommodation layer

L. Desplanque,[1] S. El Kazzi,[1] C. Coinon,[1] S. Ziegler,[2] B. Kunert,[2] A. Beyer,[3] K. Volz,[3] W. Stolz,[3] Y. Wang,[4] P. Ruterana,[4] and X. Wallart[1]
[1]*Institute of Electronics, Microelectronics and Nanotechnology, CNRS and University of Lille, Avenue Poincaré BP 60069, Villeneuve d'Ascq Cedex, France*
[2]*NAsP$_{III/V}$ GmbH, Am Knechtacker 19, 35043 Marburg, Germany*
[3]*Material Sciences Center and Faculty of Physics, Philipps-University Marburg, Hans-Meerwein-Strasse, 35032 Marburg, Germany*
[4]*CIMAP, UMR 6252 CNRS-ENSICAEN-CEA-UCBN, 6 Boulevard du Maréchal Juin, 14050 Caen Cedex, France*

(Received 6 July 2012; accepted 26 September 2012; published online 5 October 2012)

We report on the epitaxial growth of high electron mobility AlSb/InAs heterostructure on exactly oriented (001) Si substrate, using a GaP interfacial layer. The growth conditions are first optimized on GaP substrates to achieve the highest electron mobility. The influence of the Sb flux during the early stage of the GaSb buffer layer is particularly emphasized. Using these optimized growth conditions, the AlSb/InAs heterostructure is grown on a GaP/Si template obtained by metal-organic vapor phase epitaxy. An electron mobility as high as 27 800 cm^2 V^{-1} s^{-1} and 111 000 cm^2 V^{-1} s^{-1}, respectively, at 300 and 77 K is demonstrated. © *2012 American Institute of Physics*.
[http://dx.doi.org/10.1063/1.4758292]

Since the pioneering work of Kroemer's group in the early 90s, the AlSb/InAs heterostructure has demonstrated undeniable qualities for high electron mobility transistors (HEMTs). Thanks to the combination of the high conduction band offset between AlSb and InAs with the low electron effective mass in InAs, excellent transport properties have been reached on GaAs or InP substrates,[1,2] which are particularly appealing for low noise millimeter wave amplifiers and low power consumption analog devices.[3] But since a few years, as the CMOS silicon technology faces a power consumption crisis, the interest in III-V low electron effective mass materials such as InAs also increases considerably for low voltage operation MOSFET devices.[4,5] However, the monolithic integration of such III-V devices in the silicon technology requires the development of a buffer layer accommodating the large lattice mismatch (about 12% between InAs and Si) and solving the problem of anti-phase domain (APD) formation. Various solutions have been proposed such as starting the growth from an off-cut silicon substrate to promote Si double-step surfaces reducing APDs,[6] growing thick SiGe/Ge/III-V buffer layers to reduce the threading defects involved by mismatch accommodation and APDs[7] or using InSb quantum dots to filter microtwins formed at the early stages of the growth.[8]

In this paper, we demonstrate a two-step solution addressing first the problem of APDs during the epitaxial growth of a GaP interfacial layer on a (001) exactly oriented silicon substrate. The mismatch is then accommodated through a GaSb buffer layer grown on the GaP/Si template. The growth conditions at the GaSb/GaP interface leading to the highest electron mobility in the AlSb/InAs heterostructures are first determined on GaP substrates. The process is then transferred on a GaP/Si template grown by metal organic vapor phase epitaxy (MOVPE) and optimized for minimizing APD formation.[9–11]

In the first set of experiments, the growth conditions for the achievement of high electron mobility AlSb/InAs heterostructures on (001) ±0.1° GaP substrates are studied using molecular beam epitaxy (MBE) in a Riber 32P reactor. After substrate deoxidization, we used the same growth conditions for the GaP buffer layer and for the GaP surface preparation prior to GaSb deposition than the ones described in Ref. 12. As the GaSb growth starts, the reflection high energy electron diffraction (RHEED) pattern turns from a (2 × 8) surface reconstruction to a 3D one revealing the formation of islands.[13] After about 50 nm, a 2D RHEED pattern is progressively recovered as the islands coalesce. During this nucleation and coalescence stage, different Sb fluxes from 0.9 to 7.5 ML s^{-1} and growth temperature from 450 °C to 510 °C are tested, the remaining part of the 600 nm GaSb buffer layer being grown at 510 °C with a Sb flux of 2.5 ML s^{-1}. The Ga flux is fixed at 0.7 ML s^{-1} during all the experiments. The detailed stack of the Si δ-doped AlSb/InAs heterostructures grown on GaP substrate is depicted in Figure 1 (structure A). Details about the growth conditions of the heterostructure part can be found elsewhere.[2]

In a second set of experiments, a 4 × 4 cm^2 sample cleaved out from a GaP/Si template grown by MOVPE on a 300 mm (001) ±0.5° p-doped Si wafer is used as substrate for the MBE growth of the same AlSb/InAs heterostructure on a GaSb/GaP buffer layer (Figure 1, structure B). The template consists of a 1000 nm thick n-doped Si buffer layer followed by a 46 nm thick GaP nucleation film. The MOVPE growth on exactly oriented 300 mm Si substrates is carried out in a close couple showerhead reactor (Crius-R) from Aixtron SE applying triethylgallium, tertiarybuthylphosphine, and silane as group-III-, group-V-, and Si-precursors, respectively. After about 30 nm deposition, the GaP layer is free of antiphase disorder. Before the MBE growth, the GaP nucleation layer is completely pseudomorphically strained to

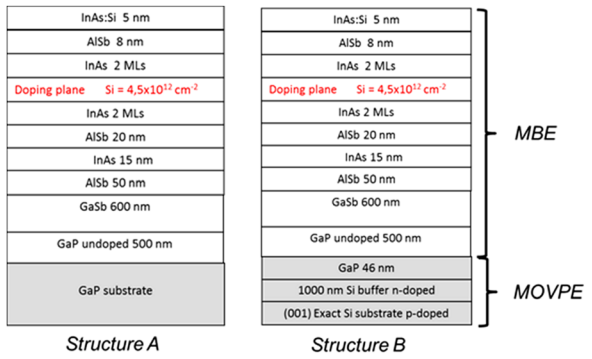

FIG. 1. Schematics of the AlSb/InAs heterostructures grown by MBE on GaP substrate (structure A) and grown by MOVPE and MBE on exactly oriented silicon substrate (structure B).

Si without any misfit- or threading dislocations. More details about the growth conditions and crystal quality are published elsewhere.[9–11]

The sample surface morphology is characterized by atomic force microscopy (AFM) using a Digital Nanoscope III system working in the tapping mode, whereas the structural properties are investigated by transmission electron microscopy (TEM) using a Jeol JEM3010 at an acceleration voltage of 300 kV and x-ray diffraction (XRD) (PANalytical X'pert PRO). Eventually, transport properties of the heterostructures are measured at room temperature (RT) and 77 K using Hall bridge mesa oriented both in [110] and [1–10] crystallographic orientations as well as a Van der Pauw configuration. Ohmic contacts to the InAs channel through the upper AlSb barrier are obtained by alloying indium contacts. For the sample grown on p-doped silicon substrate, a careful annealing process of indium contacts at 180 °C for 2 min ensures ohmic contacts to the channel while limiting indium diffusion and avoiding contact to the n-doped Si layer that could "short-circuit" the InAs channel.

Figure 2 displays typical AFM images of samples grown on GaP (structure A). The sample grown at 450 °C with a 2.5

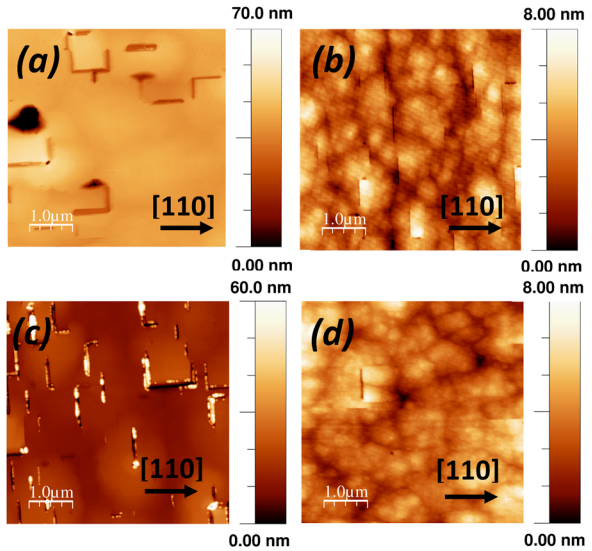

FIG. 2. AFM images of AlSb/InAs heterostructures grown on GaP substrates for a GaSb nucleation layer grown at 510 °C (a) and 450 °C (b) with a Sb flux of 2.5 ML s^{-1} at 510 °C with a Sb flux of 7.5 ML s^{-1} (c) and at 450 °C with a Sb flux of 0.9 ML s^{-1} (d). Bright spots on image c are due to AlSb oxidization within the trenches.

ML s^{-1} Sb flux (Fig. 2(b)) exhibits the formation of trenches oriented in the [1–10] direction. This behavior is very similar to that previously observed[14] where these trenches originate from twinning defects formed at the initial nucleation and coalescence stages of AlSb islands on GaAs. It has been attributed to the large Sb overpressure during the initial growth steps of AlSb on GaAs. We have demonstrated recently that Sb flux and growth temperature play a crucial role in the formation of GaSb islands on GaP too.[12] A high Sb overpressure during the initial stage of the GaSb growth results in the formation of [110] elongated islands fully relaxed by a periodic array of interface misfit dislocations (MD) and exhibiting {111} facets. The coalescence of the {111} advancing facets of the incoherent islands can result in the formation of twinning defects. As a consequence, even if a high Sb overpressure promotes the relaxation of GaSb islands, it also delays the island coalescence and induces microtwins.

For the samples grown at 510 °C (Fig. 2(a)), the morphology is slightly different since trenches oriented in the [110] direction also appear and are connected to trenches oriented in the [1–10] direction. This kind of defects is dominant at moderate Sb flux, whereas most of the defects at large Sb flux are [1–10] trenches (Fig. 2(c)). At this higher temperature (510 °C) where strong Sb reevaporation occurs, the resulting too low Sb/Ga flux ratio causes stacking faults accommodating the strain in individual islands.[12] These stacking faults are probably the origin of the "bidirectional" trenches observed at the surface of AlSb/InAs heterostructures.

As a consequence, a trade-off between GaSb relaxation and rapid island coalescence can be found by reducing both the growth temperature and the Sb flux during the nucleation layer. After full coalescence of the GaSb layer, the Sb flux and growth temperature can be simultaneously increased to improve surface roughness. Under these conditions, the heterostructure grown on GaP for which the GaSb nucleation layer is grown at 450 °C with an Sb flux of 0.9 ML s^{-1} exhibits a smooth surface with nearly no more trenches (RMS value of 0.8 nm) (Fig. 2(d)).

Figure 3 displays the results of Hall measurements performed on the heterostructures grown on GaP substrates for different Sb fluxes and growth temperatures during the 50 nm GaSb nucleation layer. For all the heterostructures, a sheet carrier density from 1.5 to 1.7×10^{12} cm^{-2} is measured. As can be seen in Figure 3(a), the Sb overpressure has a strong influence on the electron mobility. At 510 °C, a 1.4 ML s^{-1} Sb flux results in a poor electron mobility (about 10 000 cm^2 V^{-1} s^{-1}). This is related to the large Sb reevaporation on the surface at this temperature, the effective Sb/Ga flux ratio being hardly higher than unity, leading to a strong degradation of the surface morphology. This is improved by increasing the Sb flux to 2.5 ML s^{-1} but a too high Sb flux (7.5 ML s^{-1}) leads again to electron mobility degradation in the InAs channel. At lower growth temperature, this mobility decrease is observed for a 2.5 ML s^{-1} Sb flux since the Sb surface reevaporation is strongly reduced.

To understand this behavior, one must consider the electron mobility in the [110] and in the [1–10] orientations (Figure 3(b)) since the Sb flux does not affect in the same way the electron mobility in both directions. These

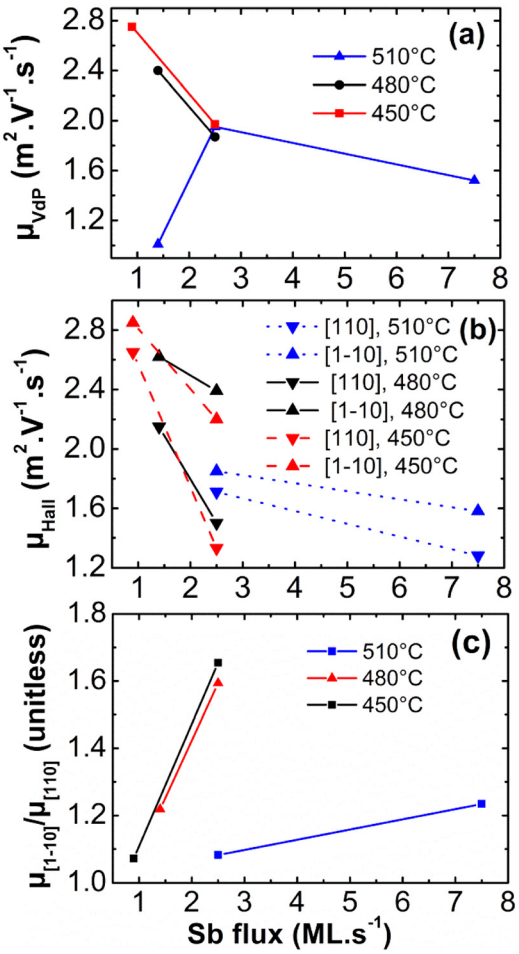

FIG. 3. Transport measurements on the heterostructures grown on GaP substrates with different temperatures and Sb fluxes during the first 50 nm of the GaSb buffer layer: (a) room temperature Van der Pauw electron mobility (μ_{VdP}), (b) Hall Bridge measurements (μ_{Hall}), and (c) anisotropy of electron mobility deduced from Figure 3(b).

variations can be qualitatively explained by the AFM observations of Figure 2. Increasing the Sb flux at a given temperature affects more severely the [110] electron mobility due to the increasing density of [1–10] oriented trenches, resulting in a higher electron mobility anisotropy (Figure 3(c)). At a fixed Sb flux, increasing the growth temperature tends to reduce this anisotropy for two reasons: (1) the effective Sb flux is reduced as Sb reevaporation is larger which decreases the [1–10] trench density and (2) the electron mobility in the [1–10] direction is also degraded due to the formation of "bidirectional" trenches.

To get a more quantitative description, the mean distance between these different trenches is estimated from their density measured on $10 \times 10\,\mu m^2$ AFM images. Those distances are in a range comparable with the electron mean free path. Figure 4 shows the correlation between the evolution of those distances and that of the electron mobility for a fixed Sb flux. It confirms that increasing the growth temperature (1) improves the electron mobility in the [110] direction as it reduces the trench density in the [1–10] direction and (2) promotes the formation of "bidirectional" trenches affecting the electron mobility in both crystallographic orientations. One can notice that for the sample grown at low temperature for which no trench in the [110] direction has been observed

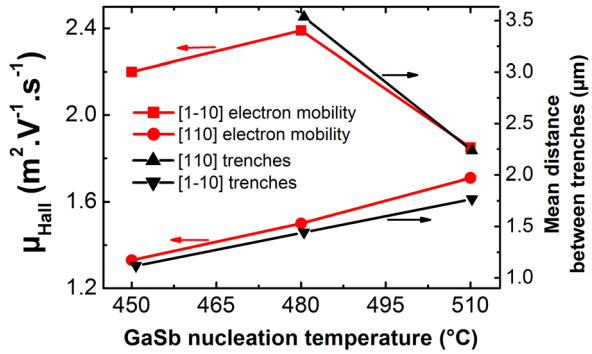

FIG. 4. Hall Bridge measurements in the [110] (circles) and [1–10] (squares) orientations for a Sb flux of 2.5 ML s^{-1} and different temperatures during the GaSb nucleation layer on GaP substrate and mean distance between [110] (up-triangles) and [1–10] (down-triangles) trenches evaluated from the trench density measured by AFM.

the large density of [1–10] trenches also affects in a lower extend the electron mobility in the trench direction.

As a consequence, the optimized conditions for the surface morphology correspond to the best transport properties and the heterostructure grown on GaP substrate for which the GaSb nucleation layer is grown at 450 °C with an Sb flux of 0.9 ML s^{-1} exhibits a Van der Pauw electron mobility of 27 800 and 120 000 $cm^2\,V^{-1}\,s^{-1}$ at 300 K and 77 K, respectively, for a sheet carrier density of $1.5 \times 10^{12}\,cm^{-2}$.

Using these optimized growth conditions, the same heterostructure is grown on a GaP/Si template grown by MOVPE. AFM (not shown) reveals a very smooth surface exhibiting a RMS value of only 0.8 nm on a $5 \times 5\,\mu m^2$ image. With a larger scale observation, a trench density in the low $10^6\,cm^{-2}$ has been estimated. Using XRD, the reciprocal space mapping (RSM) of the sample (not shown) allows deducing strain relaxation. This analysis reveals a fully relaxed GaP layer and a 101% strain relaxation in both directions for the GaSb one with parallel and perpendicular mismatches with Si of 12.44% and 12.07%, respectively (the theoretical one is 12.24%). This tensile strain in the

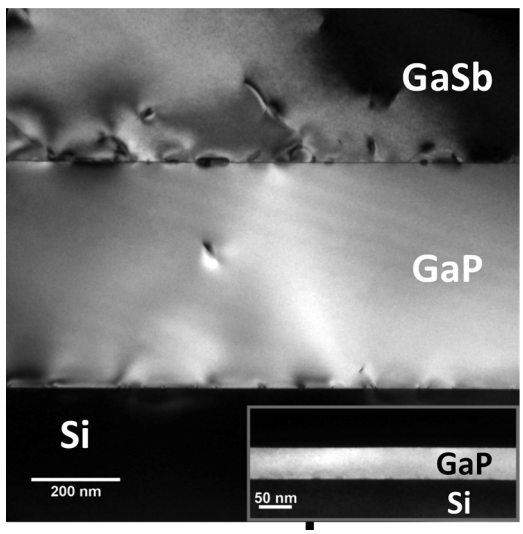

FIG. 5. 002 dark field cross section of the GaSb/GaP/Si template. Relaxation defects at the GaP/Si interface are induced by the growth of the 500 nm thick GaP buffer layer. The inset shows the GaP nucleation layer prior to the MBE deposition.

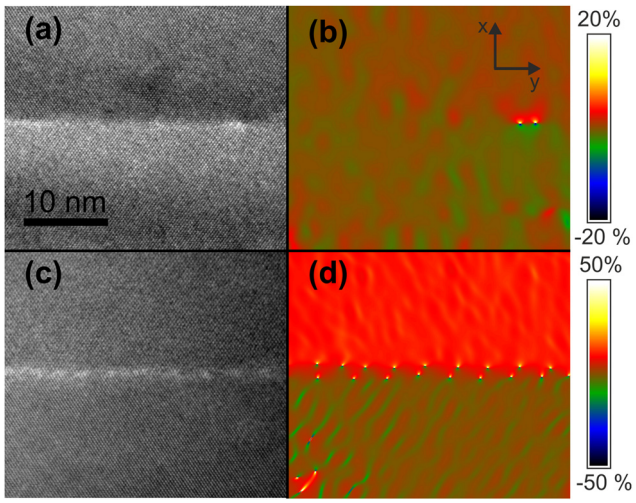

FIG. 6. HRTEM cross sections of the GaP/Si interface (a) and the GaSb/GaAs interface (c) and their associated ε_{yy} component of the strain tensor (respectively b and d).

GaSb layer can be explained considering the different expansion coefficients of GaSb ($7.75 \times 10^{-6}\,K^{-1}$) and Si ($2.6 \times 10^{-6}\,K^{-1}$). Finally, the InAs layer appears tensile strained to the GaSb buffer.

Figure 5 displays the TEM dark-field cross section of the whole structure on silicon, whereas the inset shows the GaP/Si template before MBE overgrowth. As can be noticed, it is hard to identify any APDs in the GaP nucleation layer. Nevertheless, APDs that could form at the GaP/Si interface will rapidly self-annihilate within the first 30 nm of GaP and no disorder defects reaching the GaSb/GaP interface can be observed. The high resolution TEM (HRTEM) image of the GaP/Si interface (Figure 6(a)) and the projection of the strain field along the growth direction (ε_{yy}) (Figure 6(b)) deduced from the geometric phase analysis of HRTEM images[15] reveal interface MD. These relaxation defects are induced by the MBE growth of an additional 500 nm thick GaP buffer layer. Concerning the GaSb/GaP interface, most of the mismatch is accommodated by closely spaced 60° MDs[16] resulting in a regular array with a period of about 4 nm (Figures 6(c) and 6(d)). Some imperfections of this MD array result in the formation of few threading dislocations. However, no microtwins, much more detrimental for electron mobility in the InAs channel,[14] can be observed.

Hall measurements performed on this heterostructure result in a RT Van der Pauw electron mobility of 27 800 $cm^2\,V^{-1}\,s^{-1}$ with a sheet carrier density of $1.5 \times 10^{12}\,cm^{-2}$. At 77 K, the electron mobility increases up to 111 000 $cm^2\,V^{-1}\,s^{-1}$ without almost any anisotropy confirming the high quality of the InAs channel and its usefulness for the realization of high speed and low power consumption electronic devices.

In conclusion, we have shown that high quality AlSb/InAs heterostructures can be grown on an exactly oriented silicon substrate by successively treating the problems of antiphase domain formation and lattice mismatch accommodation with a GaSb/GaP/Si template. Reducing the growth temperature and the Sb flux during the nucleation layer of GaSb on GaP is found to improve the electron mobility in the InAs channel. Using these optimized growth conditions, an electron mobility as high as 27 800 $cm^2\,V^{-1}\,s^{-1}$ at room temperature and 111 000 $cm^2\,V^{-1}\,s^{-1}$ at 77 K is demonstrated.

This work was supported by the national research agency (Contract Nos. ANR-08-NANO-022 and ANR-2010-VERS-016-01) and the German Science Foundation (DFG) (Project Nos. VO805/4 and VO805/5).

[1]G. Tuttle, H. Kroemer, and J. H. English, J. Appl. Phys. **65**, 5239 (1989).
[2]L. Desplanque, D. Vignaud, and X. Wallart, J. Cryst. Growth **301–302**, 194 (2007).
[3]B. R. Bennett, R. Magno, J. B. Boos, W. Kruppa, and M. G. Ancona, Solid-State Electron. **49**, 1875 (2005).
[4]J. Del Alamo, Nature **479**, 317 (2011).
[5]H. Ko, K. Takei, R. Kapadia, S. Chuang, H. Fang, P. W. Leu, K. Ganapathi, E. Plis, H. S. Kim, S.-Y. Chen, M. Madsen, A. C. Ford, Y.-L. Chueh, S. Krishna, S. Slahuddin, and A. Javey, Nature **468**, 286 (2010).
[6]S. H. Huang, G. Balakrishnan, A. Khoshakhlag, L. R. Dawson, and D. L. Hufaker, Appl. Phys. Lett. **93**, 071102 (2008).
[7]Y. C. Lin, H. Yamaguchi, E. Y. Chang, Y. C. Hsieh, M. Ueki, Y. Hirayama, and C. Y. Yang, Appl. Phys. Lett. **90**, 023509 (2007).
[8]K.-M. Ko, J.-H. Seo, D.-E. Kim, S.-T. Lee, Y.-K. Noh, M.-D. Kim, and J.-E. Oh, Nanotechnology **20**, 225201 (2009).
[9]I. Németh, B. Kunert, W. Stolz, and K. Volz, J. Cryst. Growth **310**, 1595–1601 (2008).
[10]K. Volz, A. Beyer, W. Witte, J. Ohlmann, I. Németh, B. Kunert, and W. Stolz, J. Cryst. Growth **315**(1), 37 (2011).
[11]A. Beyer, J. Ohlmann, S. Liebich, H. Heim, G. Witte, W. Stolz, and K. Volz, J. Appl. Phys. **111**, 083534 (2012).
[12]S. El Kazzi, L. Desplanque, C. Coinon, Y. Wang, P. Ruterana, and X. Wallart, J. Appl. Phys. **111**, 123506 (2012).
[13]S. El Kazzi, L. Desplanque, C. Coinon, Y. Wang, P. Ruterana, and X. Wallart, Appl. Phys. Lett. **97**, 192111 (2010).
[14]L. Desplanque, S. El Kazzi, J.-L. Codron, Y. Wang, P. Ruterana, G. Moschetti, J. Grahn, and X. Wallart, Appl. Phys. Lett. **100**, 262103 (2012).
[15]M. J. Hÿtch, E. Snoeck, and R. Kilaas, Ultramicroscopy **74**, 131 (1998).
[16]Y. Wang, P. Ruterana, S. Kret, J. Chen, S. El Kazzi, L. Desplanque, and X. Wallart, Appl. Phys. Lett. **100**, 262110 (2012).